

Structural transition in a fluid of spheroids: a low-density vestige of jamming

Supplementary Information

A. P. Cohen,¹ S. Dorosz,² A. B. Schofield,³ T. Schilling,² and E. Sloutskin¹

¹*Physics Department and Institute of Nanotechnology & Advanced Materials, Bar-Ilan University, Ramat-Gan 5290002, Israel*

²*Research Unit for Physics and Materials Science,*

Université du Luxembourg, L-1511 Luxembourg, Luxembourg

³*The School of Physics and Astronomy, University of Edinburgh, Edinburgh EH9 3JZ UK*

(Dated: February 7, 2016)

PREPARATION AND CHARACTERIZATION OF PROLATE COLLOIDAL SPHEROIDS

To prepare prolate ellipsoidal colloids, we uniaxially stretch simple colloidal spheres, following the procedure[4,5,18,21] which was used in the past with polystyrene[20] and poly(methylmethacrylate) (PMMA) particles stabilized by a grafted layer of PMMA-g-PDMS [poly(dimethylsiloxane)] copolymer. Our initial spherical colloids are made of PMMA and coated by a sterically-stabilizing layer of polyhydroxystearic acid (PHSA). The thickness of the PHSA monolayer[38] is ~ 10 nm, such that the interparticle potential between the initial colloids is closely approximated by the hard sphere model. The reason for choosing PMMA, rather than polystyrene or inorganic materials, is that the density and the refractive index of PMMA can be matched by mixtures of common organic solvents to form stable suspensions, where light scattering is minimized for confocal imaging deep into the bulk of the sample. The initial spheres are fluorescently labeled by the Nile Red dye, for confocal measurements. The diameter of the initial spheres is $\sigma_s = 2.4 \mu\text{m}$, as determined by static and dynamic light scattering. The polydispersity of the initial spheres is below 4%, measured by scanning electron microscopy (SEM). To characterize the size and the shape of the particles[5], we deposit them from hexane onto a clean aluminum substrate. SEM images are then obtained at 30 keV, employing the Quanta Inspect (FEITM) setup.

For the stretching of the colloidal spheres[4,5,18,21], we suspend these spheres in a 25% (w/w) solution of hydroxy terminated PDMS (typical molecular weight $M_n = 10^5$, Sigma-Aldrich) in hexane (BioLab, AR > 96%). The volume fraction of spheres in this mixture is low, $\phi \approx 0.03$. Next, a cross-linking agent, trimethylsilyl terminated poly(dimethylsiloxane-co-methylhydrosiloxane) ($M_n = 950$, Sigma-Aldrich) and a catalyst [tin(II) 2-ethylhexanoate, Sigma-Aldrich, $\sim 95\%$] are added to polymerize the PDMS. The weight fractions of the cross-linking agent and the catalyst are 6×10^3 and 8×10^3 , respectively. Immediately after the introduction of the cross-linking agent and the catalyst, the suspension is poured onto a rectangular mold, so that a $\sim 1\text{mm}$ -thick composite rubber film forms in the mold. To avoid trapping of small air volumes in the rubber, the procedure is

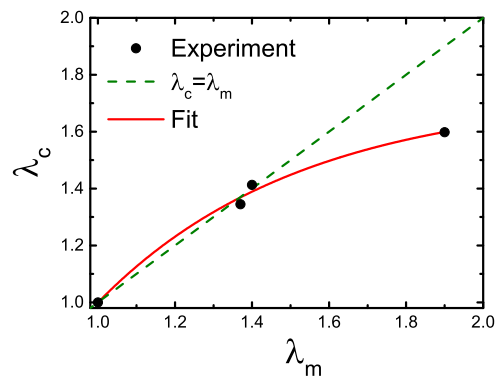


FIG. 1. The extension ratio of the PMMA colloids λ_c (scatter), is shown as a function of the extension ratio of the composite PDMS matrix λ_m . The non-linear behavior of $\lambda_c(\lambda_m)$ indicates that increasingly large strains of PDMS are needed to stretch the colloids to a high aspect ratio. Thus, the brittleness of the PDMS matrix limits the achievable t values of the colloids. Green dashes correspond to a perfect match between the strains of PDMS and PMMA, $\lambda_c = \lambda_m$. A phenomenological fit (see text) is shown in a red line.

carried out in vacuum[19], at ~ 1 mTorr. After a curing time of ~ 13 hrs, the films are post-cured for 2 hrs in an oven, pre-heated to 120°C . The rubber is then uniaxially stretched to a desired length inside an oven, at $T = 165^\circ\text{C}$, above the glass transition temperature of PMMA. For the stretching process to be accurate and reproducible, for minimization of film tearing, and in order to reduce the shape polydispersity of the resulting ellipsoids, we have constructed a computerized stretching device. This device, mounted inside an oven, is capable of stretching the films at sufficiently slow and uniform rates, $< 70 \mu\text{m/s}$. The door of our oven is equipped by a glass window, allowing the stretching process to be followed visually in real time.

Assuming that the volume of an individual particle is conserved in the stretching process, the aspect ratio t of the particle is a function of the elongation $\delta\sigma$ of its diameter: $t = (1 + \delta\sigma/\sigma_s)^{3/2}$. Thus, the extent of stretching of the PDMS matrix, with the spheres in it, determines the aspect ratio of the ellipsoids. Importantly, the extension ratio of the PMMA colloids $\lambda_c = (\sigma_s + \delta\sigma)/\sigma_s$

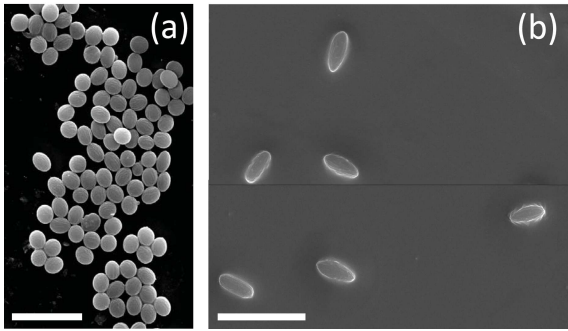


FIG. 2. SEM images of prolate colloidal ellipsoids, for the PDMS matrix stretched to an extension ratio of (a) $\lambda_m = 1.4$, (b) $\lambda_m = 1.9$. Note, the particles in panel (a) are oriented at different angles to the substrate, so that the apparent aspect ratios are smaller than the actual ones. Panel (b) was obtained by stitching of two separate SEM images, as marked by the horizontal black line.

is in general deviating from that of the PDMS matrix, $\lambda_m = (l + \delta l)/l$; here l is the initial length of the matrix, stretched to a length of $(l + \delta l)$. The experimental $\lambda_c(\lambda_m)$ relation is shown in Fig. 1 (black symbols), exhibiting a significant deviation from the naïve $\lambda_c = \lambda_m$ (green dashes). We can fit the experimental data by a phenomenological expression $\lambda_c = 1.73 - 4.89 \exp(-\lambda_m/0.53)$ (red line in Fig. 1). The observed $\lambda_c(\lambda_m)$ indicates that for large extension ratios, the strain of PMMA colloids is much smaller than that of the composite PDMS matrix, as if the PMMA exhibits a strain stiffening response.

Two typical SEM images of the ellipsoids, as obtained by the described stretching procedure, are shown in Fig. 2. Similar SEM images are employed to measure the distribution $P(t)$ of the aspect ratios of the colloids. Particle inclination angles, with respect to the (roughly) horizontal substrate, make them appear shorter in SEM images[5]. Fortunately, the volumes of our ellipsoids, obtained by volume-conserving stretching of monodisperse spheres, are almost perfectly monodisperse. Moreover, our particles are prolate spheroids; as such, they are symmetric under rotation about their long axis. Therefore, the minor axis of a particle b can be measured quite accurately by SEM, being independent of the inclination angle of the particle with respect to the substrate. We obtain the aspect ratio and the inclination angle of each individual particle in our SEM images, based on the known volume of the initial spheres ($v = 7.24 \mu m^3$) and the minor axis length b of the given particle, measured by SEM: $t = 6v\pi^{-1}b^{-3}$. The distribution $P(b)$, based on ~ 100 SEM images of colloidal particles, is shown in solid symbols in Fig. 3 for two different λ_c values. The peak position of the Gaussian fit (not shown) to the symmetric part of these $P(b)$ yields $t = 1.68 \pm 0.06$ for Fig. 2(a) and Fig. 3(a); $t = 2.02 \pm 0.06$ is obtained for Fig. 2(b) and Fig. 3(b).

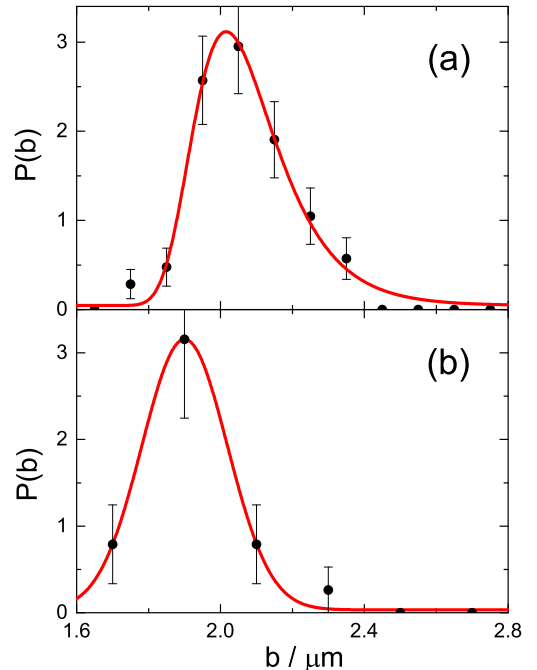


FIG. 3. Distributions of the minor axes lengths b of colloidal ellipsoids, as obtained by SEM for: (a) $\lambda_m = 1.4$, (b) $\lambda_m = 1.9$, corresponding to Fig. 2(a) and Fig. 2(b), respectively. The distribution peaks at $b = 2.02 \mu m$ for (a) and at $b = 1.68 \mu m$ for (b), corresponding to $t = 1.68 \pm 0.02$ and $t = 2.02 \pm 0.02$, respectively. The solid curves are fits by the Gumbel probability density function.

PARTICLE LOCATION ALGORITHM

Our algorithm for the detection of particle center positions and orientational angles is based on the PLuTARC algorithm, as also on the well-known algorithm of Crocker and Grier[41], previously used for tracking of colloidal spheres[39-40]. The algorithm, implemented in C/C++, takes as an input a three-dimensional stack of confocal slice images through the sample. The output consists of a list of (x,y,z) particle center coordinates and orientational angles.

The algorithm includes three stages. In the first stage, each individual two-dimensional (2D) confocal slice is analyzed. The slice is processed, so that the fluorescent colloids appear as bright, well-separated features on a dark background. A two-dimensional slice through an ellipsoidal particle is an ellipse. The center positions and the orientational angles of all such ellipses, in each of the two-dimensional slices, are measured. To find the orientational angles, we calculate the covariance matrix of the fluorescent intensity distribution at each of the particle

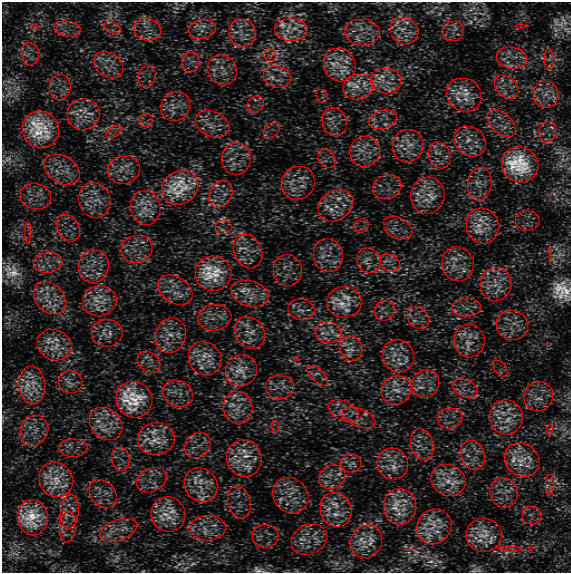


FIG. 4. A raw confocal image (2D slice, $42.4 \times 42.4 \mu\text{m}^2$) through a suspension of ellipsoids ($t = 1.68$, $\phi = 0.21$). The positions and the orientations of the particles, as detected by the first stage of our algorithm are marked by red ellipses. Note, all particles which are not perfectly parallel to the optical slice appear more rounded than they actually really are. Particles located next to the edges are excluded from the analysis, to avoid biasing of their centers by edge effects.

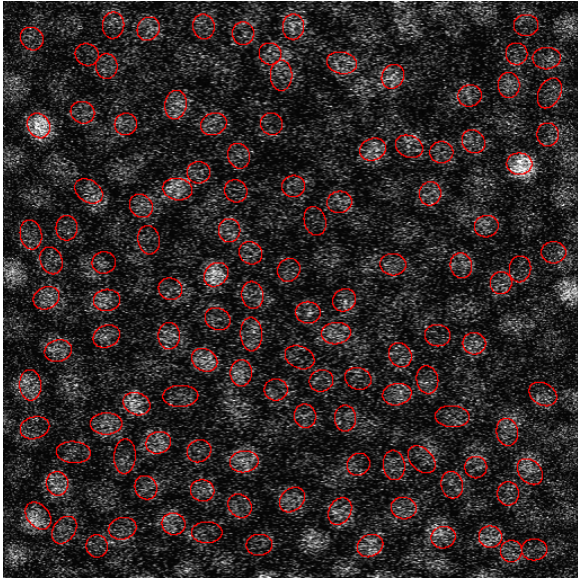


FIG. 5. A raw confocal image (2D slice, $42.4 \times 42.4 \mu\text{m}^2$) through a suspension of ellipsoids ($t = 1.68$, $\phi = 0.21$). The ellipses calculated by our algorithm from the full (3-stage) 3D reconstruction of the sample are marked in red ellipses. Note, some particles located outside of the focal plane are still visible in the image; those particles are dimmer than the rest and do not appear in the reconstruction. Particles located next to the edges are excluded, as in Fig. 4.

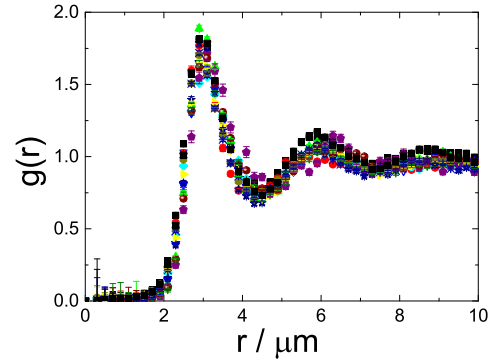


FIG. 6. The radial distribution functions (RDF) obtained from 2D slices, at different positions within the sample (different symbols), perfectly overlap. Here the aspect ratio and the volume fraction of the particles are $t = 1.68$ and $\phi = 0.21$, respectively.

positions. By diagonalization of the covariance matrices, the orientations of all elliptical slices through each of the colloids are obtained. The success of this procedure is demonstrated in Fig. 4, where the detected particle positions and orientations (red ellipses) are overlaid on top of the raw confocal slice image, for visual examination. The second stage of the algorithm links between centers of ellipses belonging to different slices, based on the lateral distance between their (x, y) coordinates and on the orientation of the ellipses. The third stage finds the direction of each ellipsoid in three dimensions. For that purpose, for each ellipsoid we retrieve from all the relevant confocal slices the three dimensional (3D) matrix of fluorescence intensity $I(x, y, z)$. The corresponding covariance matrix is then diagonalized, yielding the 3D orientation of the ellipsoid[42].

We visually examine the detected positions and orientations. For that, our codes use the reconstructed coordinates (x, y, z) and orientations (θ, ϕ) of the particles to calculate the appearance of (an elliptical cut through) each particle in each of the confocal slices. These calculated ellipses are overlaid on top of the raw confocal images, allowing the quality of the full 3D reconstruction to be assessed by visual examination (see Fig. 5).

We use the detected particle positions (x, y) in each slice (obtained in the first stage of the algorithm) to compute the radial distribution function (RDF). The RDF is then averaged over all slices to improve the statistics. The RDFs obtained at different positions within the sample perfectly overlap, as demonstrated by solid symbols in Fig. 6. The full 3D particle positions (x, y, z) , obtained in the second stage of the algorithm, yield similar $g(r)$ as well.

To determine the local volume available for each individual particle, we carry out the Voronoi tessellation of our sample, employing the Qhull software[43]. To es-

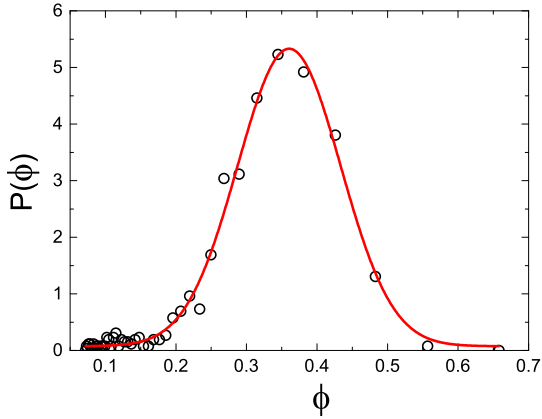


FIG. 7. A typical distribution of local volume fractions ϕ in a fluid of colloidal ellipsoids.

to estimate the local volume fraction ϕ in a suspension of prolate colloidal ellipsoids, we divide the single-particle volume $v = \pi t b^3/6$ by the volume V_V of the corresponding Voronoi cell, $\phi = v/V_V$ (see Fig. 7). $P(\phi)$ peak position provides an accurate estimate for the actual ϕ in the suspension[44].

COMPUTER SIMULATIONS

Fluids of hard ellipsoids

Monte Carlo simulations of hard ellipsoids were carried out at fixed particle number $N = 17496$, volume V and temperature T . The trial moves consisted of particle translations and rotations with a maximal distance of $1.210^{-3}b$ for the translation move and a maximal rotation by 0.42° . We sampled all data over several self diffusion times $\tilde{\tau}$ (3-5 $\tilde{\tau}$ for the higher packing fractions and up to 20 $\tilde{\tau}$ for the lower packing fractions); here $\tilde{\tau}$ is the translational long-time self-diffusion time, i.e. the time an ellipsoid needs to diffuse over the length of its equatorial diameter. The simulated $g(r)$ are in a perfect agreement with the ones obtained numerically, employing the approximate Percus-Yevick (PY) closure to solve the Ornstein-Zernike equation for hard ellipsoids[24] (see Fig. 8). Our PY-generated structure factors are also in an excellent agreement with the molecular dynamics simulations[45].

Fluids of soft dipolar particles

Molecular dynamics (MD) simulations of dipole-bearing particles [Fig. 4(b) of the main text] were carried out employing LAMMPS[46]. In addition to the

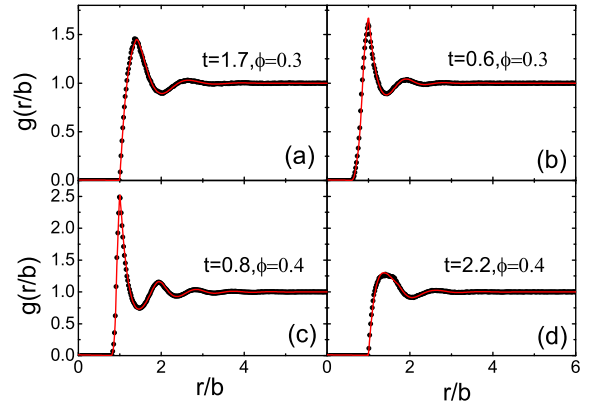


FIG. 8. The radial distribution functions of fluids of hard spheroids, obtained by Monte Carlo simulations (symbols) are perfectly matched by the PY-theoretical calculations (solid curves). The data are shown for different volume fractions ϕ and aspect ratios t (see labels), both for the oblate and the prolate particles. The r values are normalized by the equatorial axis of the ellipsoids b .

dipole-dipole interactions u_{pp} , the particles interact via a repulsive truncated Lennard-Jones (Weeks-Chandler-Andersen) potential:

$$u_{LJ}(r) = \begin{cases} 4\epsilon[(\sigma/r)^{12} - (\sigma/r)^6 + 1/4] & r < r_c = 2^{1/6}\sigma \\ 0 & r \geq r_c \end{cases} \quad (1)$$

The parameters σ and ϵ can be used to define convenient MD length and energy units, respectively, with mass expressed in terms of the sphere mass, and the MD temperature unit T obtained by setting $k_B = 1$. The dipole-dipole interaction is given by: $u_{pp} = r^{-3} \vec{p}_i \cdot \vec{p}_j - 3r^{-5} (\vec{p}_i \cdot \vec{r})(\vec{p}_j \cdot \vec{r})$, where \vec{p}_i and \vec{p}_j are the dipole moments of the i -th and the j -th particles, respectively; u_{pp} is cut off at $r = 3\sigma$. The simulations involve systems of 1000 particles, running at $T = 0.33$. Periodic boundaries are used in all three dimensions and the simulation cell size is determined by the overall number density, $\rho^* = 0.4$, in Lennard-Jones units.

SCALING OF r_p/L : PHENOMENOLOGICAL ARGUMENTS

In the main text, the non-monotonic variation of r_p/L with the aspect ratio is explained by phenomenological arguments, which single out four possible regimes: (a) $t \gg 1$; (b) $t \ll 1$; (c) $t \leq 1$; (d) $t \geq 1$. These four regimes are schematically depicted in Fig. 9, where the particles are yellow and their effective occupied volume is denoted by black ellipses and circles.

In Fig. 9(a-b), the particles have their long axes

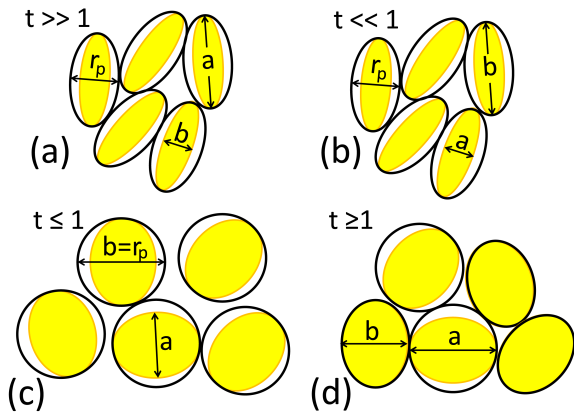


FIG. 9. Schematic representation of four different regimes of packing in fluids of spheroids: (a) $t \gg 1$; (b) $t \ll 1$; (c) $t \leq 1$; (d) $t \geq 1$. Particle cross-sections are shown in yellow; the excluded volumes are depicted as black ellipses and circles. r_p is the position of the principal peak of the $g(r)$; a is the symmetry axis.

aligned, locally, in parallel. Importantly, while for the prolate particles [Fig. 9(a)] the long axis is the polar one,

for the oblate ones [Fig. 9(b)] the equatorial axes are the longer ones. The densest packing[6] of the effective volumes in Fig. 9(a-b), at a volume fraction of ~ 0.77 , yields $r_p = (0.77/\phi)^{1/2}b$ for the prolate particles and $r_p = (0.77/\phi)a = (0.77/\phi)bt$ for the oblate ones. Here $\phi = N\pi tb^3/6V$ is the volume fraction of N colloidal spheroids in volume V ; the expressions for r_p result by noting that the number density of particles N/V is equal to that of their excluded volumes, while the volume fractions are ϕ and 0.77, respectively. The obtained r_p are then divided by $L = bt^{1/3}$, to obtain the dash-dotted and dash-double-dotted lines in Fig. 2(a) of the main text.

The other two regimes, corresponding to almost-spherical oblate and prolate particles, are shown in Fig. 9(c) and Fig. 9(d), respectively. In these regimes the particles rotate freely. Thus, the excluded volumes of the oblate particles are spherical [Fig. 9(c)]. The prolate particles are assumed to rotate in one plane, so that the corresponding excluded volume of a particle has a shape of an oblate ellipsoid [Fig. 9(d)]. These ellipsoidal excluded volumes are oriented randomly; for clarity of representation, all the volumes in the cartoon are shown to have their polar axis at either 0° or 90° to the image plane.